Solid State Ionics 332 (2019) 16–24

Contents lists available at ScienceDirect

Solid State Ionics

journal homepage: www.elsevier.com/locate/ssi

Diffusion couple study of the interaction between Cr_2O_3 and $MnCo_2O_4$ doped with Fe and Cu

Belma Talic[a,b], Peter Vang Hendriksen[b], Kjell Wiik[a], Hilde Lea Lein[a,*]

[a] Department of Materials Science and Engineering, Norwegian University of Science and Technology, Sem Sælands Vei 12, 7491 Trondheim, Norway
[b] Department of Energy Conversion and Storage, Technical University of Denmark, DTU Risø Campus, Frederiksborgvej 399, DK-4000 Roskilde, Denmark

ARTICLE INFO

Keywords:
Spinel oxide
Chromia
Solid oxide fuel cell
Solid oxide electrolysis
Interconnect
Corrosion
Protective layers

ABSTRACT

Manganese cobalt spinel oxides are promising coating materials for the protection of ferritic stainless steel interconnects in solid oxide fuel cell (SOFC) stacks. The interaction between such coatings and the steel is here studied using diffusion couples as a model system. The interaction between $MnCo_2O_4$, $MnCo_{1.7}Fe_{0.3}O_4$ and $MnCo_{1.7}Cu_{0.3}O_4$ spinels and Cr_2O_3 was studied in air at 900 °C. In all cases, a reaction layer rich in Co and Cr formed at the interfaces. Using Pt-particles to mark the original interface reveals that the reaction layers grow by diffusion of Co (and Mn) from the spinel oxides to the Cr_2O_3/reaction layer interface. The growth of the reaction layers followed parabolic kinetics with rate constants of $1.3 \times 10^{-5}\,\mu m^2\,s^{-1}$ for the $MnCo_2O_4/Cr_2O_3$ couple, $8.6 \times 10^{-6}\,\mu m^2\,s^{-1}$ for the $MnCo_{1.7}Fe_{0.3}O_4/Cr_2O_3$ couple, and finally $1.2 \times 10^{-4}\,\mu m^2\,s^{-1}$ for the $MnCo_{1.7}Cu_{0.3}O_4/Cr_2O_3$ couple.

1. Introduction

One of the factors currently limiting the lifetime and performance of solid oxide fuel cell (SOFC) and electrolysis stacks is degradation of the ferritic stainless steel (FSS) used as the interconnect material. When FSS is exposed to the typical SOFC operating conditions (650–900 °C in air and H_2-H_2O atmospheres) an oxide scale consisting of Cr_2O_3 and $(Mn,Cr)_3O_4$ is formed. Because of the modest electrical conductivity of these oxides, the resistance across the stack increases with time as the scale grows thicker, leading to a decrease in the stack power output [1,2]. Furthermore, the evaporation of Cr(VI)-species from the oxide scale causes degradation of the SOFC cathode [3–5]. A promising way to mitigate these issues is to coat the FSS with $(Mn,Co)_3O_4$ [6–14].

When oxidizing FSS coated with $(Mn,Co)_3O_4$ a Cr-rich $(Mn,Co,Cr)_3O_4$ reaction layer forms at the oxide scale/coating interface [7,9,10,15,16]. Formation of this reaction layer is beneficial as it limits the outward transport of Cr to the coating surface, where it could evaporate. Furthermore, diffusion of oxygen has been shown the be slower through the $(Mn,Co,Cr)_3O_4$ reaction layer than through both the $MnCo_2O_4$ coating and the thermally grown Cr_2O_3 scale [12]. This indicates that the reaction layer might be responsible for the reduced oxidation rate of $(Mn,Co)_3O_4$ coated FSS. However, the electrical conductivity of $(Mn,Co,Cr)_3O_4$ is known to decrease with increasing Cr content, from $89\,S\,cm^{-1}$ for $MnCo_2O_4$ to only $0.007\,S\,cm^{-1}$ for $Mn_{0.5}Co_{0.5}Cr_2O_4$ (800 °C) [17,18]. Thus, unless the thickness and Cr content of the $(Mn,Co,Cr)_3O_4$ layer is limited, it may contribute significantly to the area specific resistance (ASR) of the interconnect. Furthermore, as formation of $(Mn,Co,Cr)_3O_4$ consumes the coating, the growth rate of this layer will influence the lifetime of $(Mn,Co)_3O_4$ coated FSS interconnects.

The interaction between a $Mn_{1.5}Co_{1.5}O_4$ coating and the FSS Crofer 22 APU has been investigated in detail using transmission electron microscopy (TEM) [15]. The $Mn_{1.5}Co_{1.5}O_4$ coating was applied in slurry form and sintered by a two-step reduction and re-oxidation procedure before long-term oxidation in air. The diffusion of Cr in this system was reported to follow a complicated sequence of fluxes, involving outward diffusion of Cr from the alloy during coating sintering, inward diffusion of Cr during initial 250 h exposure in air, and finally again outward diffusion during long term exposure. A ca. 4 μm thick $Mn_{1.38}Co_{0.84}Cr_{0.54}Fe_{0.24}O_4$ layer had formed after 1000 h at 800 °C [15]. The steel-spinel coating interaction has also been studied using diffusion couples comprising sintered $Mn_{1.5}Co_{1.5}O_4$ and Cr_2O_3 pellets as a model system [19]. By applying Pt markers at the original interface, it was concluded that a $(Mn,Co)Cr_2O_4$ layer grows by diffusion of Co and Mn towards the $Cr_2O_3/(Mn,Co)Cr_2O_4$ interface. The growth could be described by a parabolic rate law ($l \propto (kt)^{1/2}$, where l is the thickness, k is the rate constant and t is the time) with a rate constant of $6.9 \times 10^{-5}\,\mu m^2\,s^{-1}$ at 900 °C.

* Corresponding author at: Department of Materials Science and Engineering, Norwegian University of Science and Technology, Sem Sælands Vei 12, 7491 Trondheim, Norway.
E-mail addresses: beltal@dtu.dk (B. Talic), pvhe@dtu.dk (P.V. Hendriksen), kjell.wiik@ntnu.no (K. Wiik), hilde.lea.lein@ntnu.no (H.L. Lein).

https://doi.org/10.1016/j.ssi.2019.01.008
Received 21 August 2018; Received in revised form 18 December 2018; Accepted 4 January 2019
Available online 11 January 2019

We have previously reported on the oxidation rate and time dependence of the cross scale area specific resistance (ASR) for Crofer 22 APU coated with $MnCo_2O_4$, $MnCo_{1.7}Cu_{0.3}O_4$ and $MnCo_{1.7}Fe_{0.3}O_4$ [20]. All three coatings were equally effective in reducing the oxidation rate of Crofer 22 APU in air at 900 °C. However, while a continuous and ca. 5.1 μm thick $(Mn,Co,Cr)_3O_4$ reaction layer was formed after 2000 h of oxidation with the $MnCo_2O_4$ coating, the reaction layers formed with the Fe and Cu doped coatings were not continuous and significantly thinner (their average thickness could not be accurately determined due to large variations). To investigate possible reasons for these differences, we have here studied the interaction between the coating materials and Cr_2O_3 using diffusion couples. More knowledge about the growth rate of the reaction layers and how it is influenced by doping of the coating is important for a more reliable prediction of the lifetime of spinel coated interconnects and for identifying routes for further improvement.

2. Experimental

$MnCo_2O_4$ (MC), $MnCo_{1.7}Fe_{0.3}O_4$ (MCFe) and $MnCo_{1.7}Cu_{0.3}O_4$ (MCCu) spinel powders were prepared by spray pyrolysis of aqueous-based nitrate solutions as described in detail elsewhere [18]. After calcination at 650 °C for 10 h, the powders were ball milled overnight in 100% ethanol (250 ml PE-bottle, Ø 10 mm YSZ balls), dried in a rotavapor and sieved at 250 μm. The particle size after milling was bimodal with the median (d_{50}) equal to 0.70 μm for MC, 0.63 μm for MCFe and 1.22 μm for MCCu [20]. Pellets of the spinel powders were prepared by uniaxial pressing in a Ø = 20 mm steel die at 40 MPa. The spinel pellets were sintered in flowing air at 1100 °C for 5 h and subsequently annealed at 800 °C for 12 h (2 °C min^{-1} heating and cooling rate). The annealing step was included to re-oxidize the spinel, which is partially decomposed when heated above 1050 °C in air [21,22]. Cr_2O_3 powder (Alfa Aesar, purity: 99% on basis of metals, BET surface area: 3.4 $m^2 g^{-1}$) was used in the as-received state. Cr_2O_3 pellets were prepared by uniaxial pressing in a Ø = 20 mm steel die at 40 MPa. The pressed pellets were sintered in flowing Ar-5%H_2 at 1500 °C for 2 h (3.3 °C min^{-1} heating and cooling rate). The sintered spinel and Cr_2O_3 pellets were ground with #500 SiC paper to make the faces parallel. One face was subsequently polished with diamond abrasive in successive steps down to 1 μm.

The density of the sintered pellets was determined by the Archimedes method according to ISO 5017:1998(E) using isopropanol as the immersion liquid. The phase purity of the sintered, polished pellets was checked on a Bruker D8 X-ray diffractometer (XRD) with Cu-Kα radiation. Diffractograms were recorded on rotating samples from 15 to 75° 2θ using a step size of 0.02° and a collection time of 1 s per step. The lattice parameters were determined by refinement of the XRD patterns in TOPAS (Bruker).

The interaction between the spinel oxides and Cr_2O_3 was studied by placing the polished faces of the pellets against each other to form a diffusion couple. The original interface was marked by a thin layer of colloidal Pt paint (particle size < 0.1 μm). The diffusion couple was placed between two alumina plates and a load of ca. 0.1 MPa was applied. Annealing was performed in a vertical tube furnace at 900 °C in stagnant air for 20–1000 h (heating and cooling rate 120 °C h^{-1}). The annealing temperature (900 °C) is slightly higher than the typical operating temperature of solid oxide fuel cell stacks today and was chosen in order to decrease the time necessary to form the reaction layers. Three diffusion couples (one of each spinel oxide material) were placed in the furnace simultaneously, separated by alumina plates. After annealing for 20, 150, 300, 500 or 1000 h continuously, the diffusion couples were mounted in epoxy resin, cut by a diamond saw perpendicular to the reaction interface and polished with diamond abrasive in successive steps down to 1 μm.

The thickness and composition of the reaction zone was characterized by scanning electron microscopy (SEM, Zeiss Supra 35 Field Emission SEM) and energy dispersive X-ray spectroscopy (EDX, Noran System SIX X-ray microanalysis system). EDX data were collected at an acceleration voltage of 15 kV and analyzed using the Noran System SIX software (Thermo Scientific, ver. 2.3). The collected spectra were analyzed without using a standard and the results in terms of composition must therefore be considered semi-quantitative. To avoid errors due to overlapping peaks, quantification was based on the K-lines for Cr, Mn, Co, Cu and Fe. The interaction volume for EDX was estimated by Monte Carlo simulations using the CASINO v2.42 software [23]. According to these simulations the majority of characteristic X-rays (Kα photons) will be emitted from a depth of ~1.0 μm, with a radial distribution of ~0.3 μm in $MnCo_2O_4$, and from a depth of ~1.4 μm with a radial distribution of ~0.5 μm in Cr_2O_3.

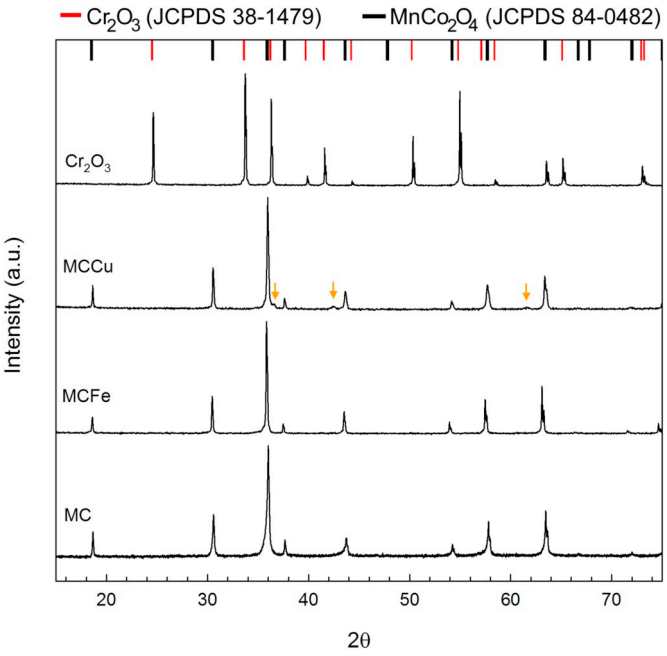

Fig. 1. X-ray diffractograms of sintered spinel (air, 1100 °C + 800 °C) and Cr_2O_3 (Ar-5%H_2, 1500 °C) pellets. Arrows highlight peaks belonging to CuO (JCPDS 78-0428).

3. Results

3.1. Characterization of starting materials

Fig. 1 shows XRD patterns of all pellets after sintering and polishing. The diffractogram of the Cr_2O_3 pellet matches the database file for Cr_2O_3 (JCPDS 38-1479). XRD patterns of the MC, MCFe and MCCu pellets can be indexed to the cubic spinel structure, with peak positions close to the database file of $MnCo_2O_4$ (JCPDS 84-0482). In the pattern for the MCCu pellet, three additional peaks are visible at ~36.5°, ~42.5° and ~61.5°. These peaks can be indexed to the cubic CuO structure (JCPDS 78-0428). The semi-quantitative weight percentage of the CuO phase is 3.4% (calculated using the Bruker DIFFRAC.EVA software).

The lattice parameters of the spinel materials after sintering were determined by a structure fit of the XRD patterns to the cubic $Fd\bar{3}m$ space group with the cation distribution[1] set to $(Co^{2+})[Co^{3+}Mn^{3+}]O_4^{2-}$. Both iron (as Fe^{3+}) and copper (as Cu^{2+}) were added to the octahedral position in place of cobalt. The determined lattice parameters were: 8.298 Å for MC, 8.346 Å for MCFe, and 8.310 Å for MCCu. Assuming the

[1] The round brackets () designate cations in tetrahedral positions, the square brackets [] designate cations in octahedral positions.

compositions are according to target, i.e. $MnCo_2O_4$, $MnCo_{1.7}Fe_{0.3}O_4$ and $MnCo_{1.7}Cu_{0.3}O_4$, the theoretical densities are 5.51 g cm^{-3}, 5.39 g cm^{-3} and 5.51 g cm^{-3}, respectively. Using these densities as a reference, the density of the sintered pellets used in the diffusion couples are 91% for MC, and 95% for MCFe and MCCu according to the Archimedes measurement. The density of the sintered Cr_2O_3 pellet is 95% (using 5.21 g cm^{-3} as the theoretical density [24]). The high density determined by the Archimedes method is confirmed by measurement of the geometric density, which was 90% for MC, 92% for MCFe, 94% for MCCu and 93% for Cr_2O_3 (average of three samples).

SEM images of the polished surfaces of the sintered spinel oxide and Cr_2O_3 pellets, confirming the high density, are included in the Supplementary Material (Fig. S1). The spinel samples were thermally etched (10 min, 1000 °C, air) after polishing to reveal the grain boundaries. The grain size is generally in the range of 1–3 μm, with the MC sample displaying slightly larger grains than the MCFe and MCCu samples.

3.2. Characterization of reaction layers

3.2.1. MC/Cr_2O_3 and MCFe/Cr_2O_3 diffusion couples

Fig. 2 shows representative cross sectional SEM backscatter electron (BSE) images and EDX line-scans of the MC/Cr_2O_3 and MCFe/Cr_2O_3 diffusion couples after 300 h at 900 °C. The results are normalized to the total cation fraction based on atomic % since analysis of oxygen content by EDX is inaccurate. The original EDX line-scan did nevertheless indicate a decreasing oxygen content from Cr_2O_3 (ca. 64 at.%) to the MC/MCFe spinel oxides (ca. 57 at.%). A single reaction layer (in the following abbreviated: RL) is formed at the MC/Cr_2O_3 (Fig. 2a) and MCFe/Cr_2O_3 (Fig. 2b) interfaces; visible in the SEM-BSE images as a medium contrast phase between the lighter MC/MCFe phases and the darker Cr_2O_3 phase. There is a significant difference in width of the two reaction layers. The composition of the RL is approximately $Co_{0.9}Mn_{0.2}Cr_{1.9}O_4$ for the MC/Cr_2O_3 diffusion couple and $Co_{0.88}Mn_{0.17}Fe_{0.05}Cr_{1.9}O_4$ for the MCFe/Cr_2O_3 diffusion couple according to the EDX analysis. The compositions are nearly constant across the RLs (± 0.1 for fraction of the different cations), as evident from the flatness of the EDX profiles. The relatively steep gradient in Cr concentration across the RL/MC and RL/MCFe interfaces indicates minimal diffusion of Cr into the MC and MCFe spinels. The Cr cation fraction in MC and MCFe is < 0.03 ca. 1 μm from the respective interfaces. Although the RL grew thicker with time (see Section 3.3), the RL composition was not noticeably different for diffusion couples annealed 20, 300, 500 and 1000 h at 900 °C.

The majority of the Pt markers were observed at the spinel/RL interface, consistent with growth of the RL at the Cr_2O_3/RL interface. In a few places, Pt makers were observed at both interfaces and at various locations within the RL, as seen in Fig. 2b. Markers observed at the MCFe/RL interface and within the RL have probably become displaced by the reaction front due to plastic flow of the oxide [25]. There was no apparent correlation between the composition and thickness of the RL and the position of the Pt markers, hence, the Pt markers do not seem to have influenced the reaction. Growth of the RL at the Cr_2O_3/RL interface is supported by the observation that this interface is wavy, while the MC/RL and MCFe/RL interfaces are typically much more smooth (see Fig. 2).

For the diffusion couples annealed for 20 h at 900 °C there was poor adherence between the spinel and Cr_2O_3 pellets after cooling to room temperature and release of the load. The reaction layer was in this case exclusively observed on the spinel oxide pellets. No Co, Mn or Fe could be detected on the Cr_2O_3 pellets by EDX. The adherence between diffusion couples annealed for 150 h at 900 °C was sufficient to allow for mounting in epoxy. Diffusion couples annealed for 500 and 1000 h were partially cracked, particularly in the MC/MCFe pellets. The MC pellets were overall more severely damaged compared to the MCFe pellets.

3.2.2. MCCu/Cr_2O_3 diffusion couple

Fig. 3 shows a representative cross sectional SEM-BSE image and EDX analysis results of the MCCu/Cr_2O_3 diffusion couple after 300 h at 900 °C. The contrast in the SEM-BSE image indicates a RL consisting of two phases. EDX analysis of the MCCu/Cr_2O_3 interface reveal that the brighter contrast phase of the RL contains more Mn and less Cr compared to the darker contrast phase. The “bands” of the brighter Mn-rich phase extend nearly all the way to the Cr_2O_3/RL interface, becoming more narrow towards this interface. This morphology is reflected in the EDX line-scan as an increase in Cr content across the RL when going from the MCCu/RL interface to the Cr_2O_3/RL interface (i.e. a larger fraction of the Cr-rich darker contrast phase towards the interface with

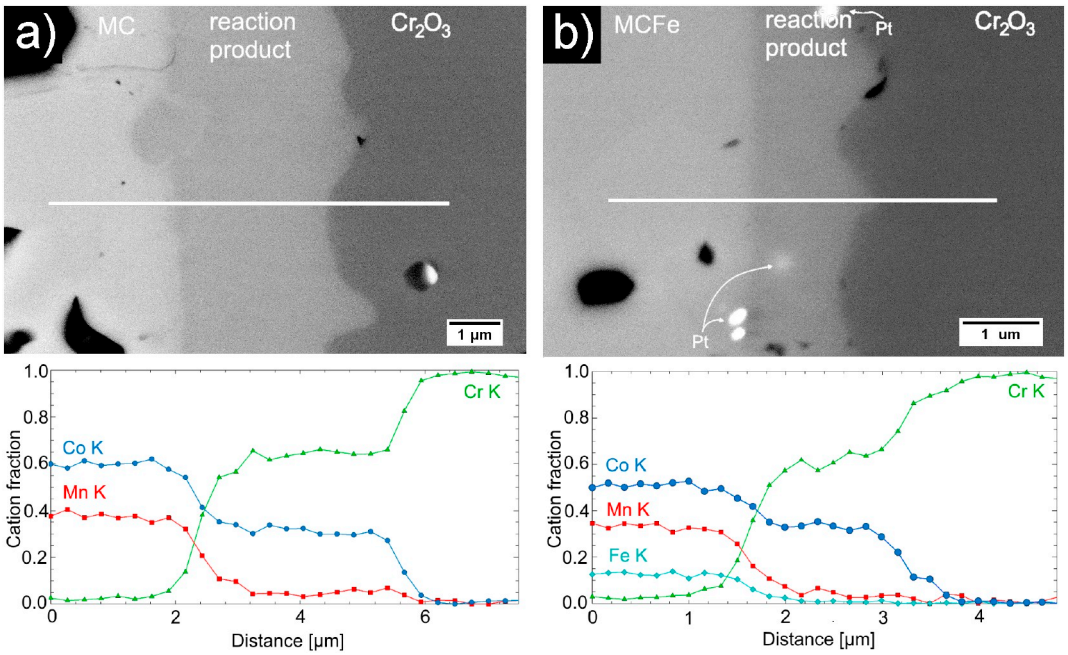

Fig. 2. SEM-BSE image and EDX line-scan of the interface of the a) MC/Cr_2O_3 and b) MCFe/Cr_2O_3 diffusion couple annealed 300 h at 900 °C. The white line in the SEM image marks the position of the EDX line-scan. The results are normalized according to the total cation content.

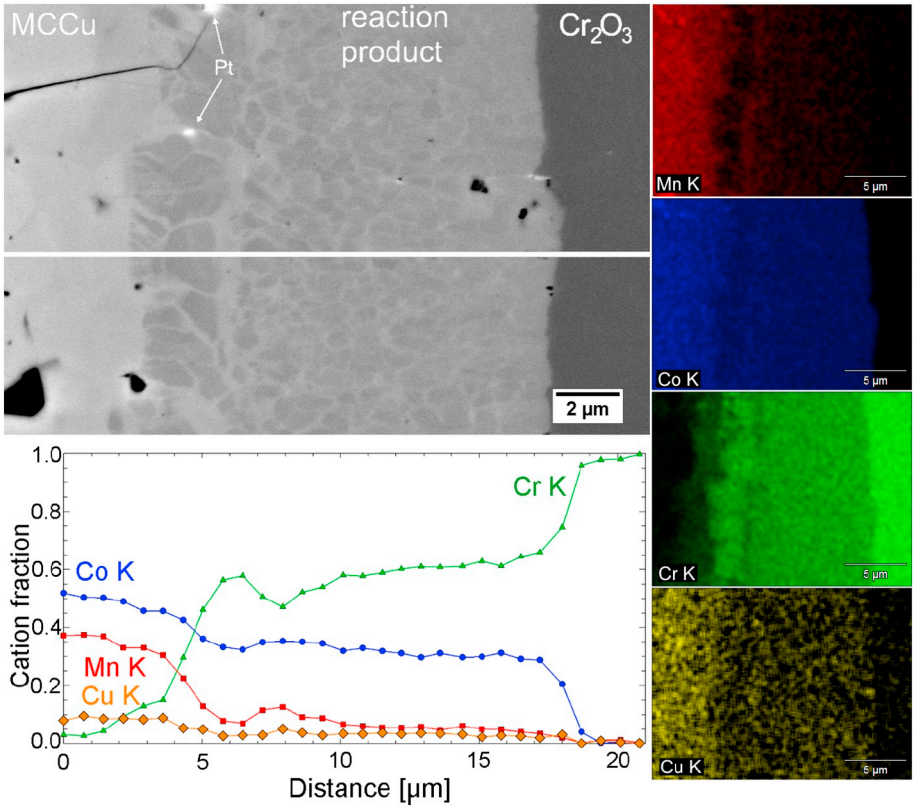

Fig. 3. SEM-BSE image and EDX linescan across interface of the MCCu/Cr_2O_3 diffusion couple annealed 300 h at 900 °C. The white line in the SEM image marks the position of the EDX line-scan. The results are normalized according to the total cation content.

Cr_2O_3). Compared to the RLs formed with the MC/Cr_2O_3 and MCFe/Cr_2O_3 diffusion couples (cf. Fig. 2), the RL formed with the MCCu/Cr_2O_3 diffusion couple has an overall lower Cr fraction and an overall higher Mn fraction. The RL additionally contains some Cu.

The Pt marker positions and EDX results indicate diffusion of Co, Mn and Cu from MCCu towards the RL/Cr_2O_3 interface, as well as some diffusion of Cr from the RL into MCCu. This is visible in the EDX line-scan as the "shoulder" in the Cr concentration profile at 2–4 µm distance.

The MCCu material sintered to the alumina plate during annealing and CuO precipitates were found close to the MCCu/alumina plate interface. A SEM image of the MCCu/alumina plate interface after 500 h at 900 °C is shown in the Supplementary Material (Fig. S2). Furthermore, a Cr and Cu rich phase (23 at.% Cr, 21 at.% Cu, 55 at.% O, < 1 at.% Co, Mn) was detected close to the outer edges of the diffusion couple and as isolated 1–3 µm sized particles along the Cr_2O_3/RL interface in the center of the diffusion couple (Fig. S3 in the Supplementary Material). No CuO was detected in proximity of the reaction layer formed between MCCu and Cr_2O_3.

All Cr_2O_3 pellets contained some 5–20 µm sized particles rich in Fe and Cr after annealing. These were typically observed in large clusters relatively far away (> 50 µm) from the spinel pellet interface. Since these secondary phases also were observed in Cr_2O_3 pellets annealed with Fe-free spinels (MC, MCCu), they are likely formed due to iron (oxide) impurities in the as-received Cr_2O_3 powder. This secondary phase has not affected the reactivity between Cr_2O_3 and the spinel oxides as no Fe was detected in the reaction layer formed between Cr_2O_3 and the MC and MCCu materials.

3.3. Kinetics of the reaction layer formation

The reaction layer thickness as a function of annealing time at 900 °C is shown in Fig. 4. The thickness of the RL was measured in areas where all layers were in contact after mounting in epoxy.[2] The MC/Cr_2O_3 diffusion couple annealed for 1000 h could not be analyzed due to extensive cracking of the sample. For the MCCu/Cr_2O_3 diffusion couples, only the thickness of the Cr-rich RL was measured.

For all three materials, the development of the reaction layer thickness with time can be described as approximately parabolic ($l \propto (kt)^{1/2}$). The parabolic growth rate constants of the RL were determined to $1.2 \times 10^{-4}\,\mu m^2\,s^{-1}$ for MCCu, $1.3 \times 10^{-5}\,\mu m^2\,s^{-1}$ for MC, and $8.6 \times 10^{-6}\,\mu m^2\,s^{-1}$ for MCFe (see Fig. S4 in the Supplementary Material). Based on the standard deviation of the RL thickness measurement, the uncertainty of the rate constant can be estimated to ca. 40% for MC, 20% for MCFe and 10% for MCCu.

4. Discussion

4.1. Interaction between MC/MCFe and Cr_2O_3

The RL formed at the interface of the MC/Cr_2O_3 and MCFe/Cr_2O_3 diffusion couples after annealing at 900 °C was essentially the same, consisting of a single layer with a composition approximately equal to $Co_{0.9}Mn_{0.2}Cr_{1.9}O_4$ for the MC/Cr_2O_3 diffusion couple and $Co_{0.88}Mn_{0.17}Fe_{0.05}Cr_{1.9}O_4$ for the MCFe/Cr_2O_3 diffusion couple (Fig. 2). The AB_2O_4 spinel structure can be described as a nearly cubic close packed arrangement of oxygen ions with 1/8 of the available tetrahedral sites occupied by the A cations and 1/2 of the available octahedral sites occupied by the B cations. Cr^{3+} is known to have a very strong preference for the octahedral (B) sites in this structure and is rarely found at the tetrahedral (A) sites under normal conditions

[2] An exception to this was for the MC and MCFe diffusion couples annealed for 20 h, where the two pellets were detached after removal from the furnace. For these pellets, the thickness of the RL in contact with the spinel was measured.

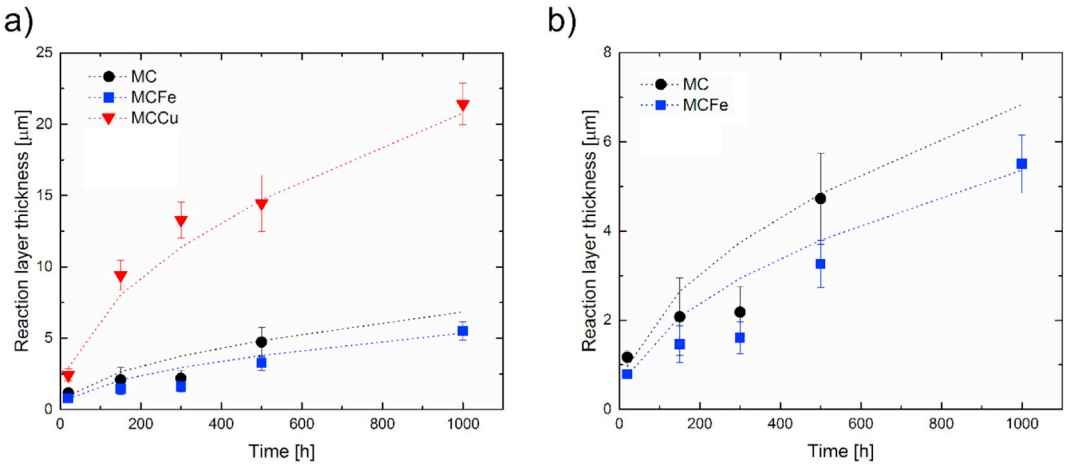

Fig. 4. Thickness of reaction layer formed between MC, MCFe, and MCCu spinels and Cr_2O_3 as a function of annealing time at 900 °C in air. The stippled lines show reaction layer thickness calculated from the derived parabolic rate constant. a) Scaled to results of MCCu/Cr_2O_3, b) Scaled to result of MC/Cr_2O_3 and MCFe/Cr_2O_3.

[26–28]. The maximum cationic fraction of Cr in spinel oxides is therefore 2/3, which is close to the fraction measured in the RL (1.9/3). These results are reasonable considering that the solubility of both Co and Mn in Cr_2O_3 is negligible [28,29] and within the solid solution of $Co_xCr_{3-x}O_4$ ($1 < x < 3$), $CoCr_2O_4$ is the composition that is thermodynamically stable over the widest range of temperature and pO_2 [30]. That is, $CoCr_2O_4$ is effectively the most stable composition.

The growth rate of the RL followed parabolic kinetics, which indicates that the rate is controlled by solid state diffusion across the growing RL. Since a majority of the Pt markers were observed at the MC/RL and MCFe/RL interfaces it may be inferred that the RL grows at the interface with Cr_2O_3 by diffusion of Co (and Mn) to this interface. When reviewing literature on diffusion in $CoCr_2O_4$ and related spinel oxides this indeed seems more probable than a mechanism involving Cr diffusion in the opposite direction. The tracer diffusion coefficients of Cr, Co, Fe and Mn have been measured at 1200 °C in $(Mn,Co)_3O_4$ and $(Mn,Co,Fe)_3O_4$ by Lu and Dieckmann [31–33], and in $(Cr,Fe)_3O_4$ by Töpfer et al. [34]. In all of these materials, Cr has a diffusion coefficient three orders of magnitude lower than that of Mn, Co and Fe. Sun [35] reported that the activation energy for Co^{2+} diffusion (51 kJ/mol) in $CoCr_2O_4$ was lower than the activation energy for Cr^{3+} diffusion (70 kJ/mol) in the temperature range of 1400–1600 °C in air. The tracer diffusion coefficients of Co, Mn, and Fe in $(Mn,Co)_3O_4$, $(Mn,Co,Fe)_3O_4$ and $(Cr,Fe)_3O_4$ are within the same order of magnitude at 1200 °C, but the diffusivity of Co is slightly higher, particularly at lower pO_2 [31–34]. The nearly flat concentration profile of Co and Cr in the RL and the waviness of the RL/Cr_2O_3 interface (Fig. 2) points to that the transport of Co through the RL is dominated by grain boundary diffusion.

The Co-to-Mn fraction in the RL is considerably higher compared to the Co-to-Mn fraction in the original MC and MCFe spinels. This is consistent with calculations by Persson et al. [36] showing that the Gibbs energy change for a mixture of Cr_2O_3, Mn_3O_4 and CoO to the equilibrium state at 900 °C becomes more negative with decreasing Mn content in the mixture. I.e. a reaction between the three components becomes thermodynamically more favorable with lower concentrations of Mn.

The RL growth rate was ca. 50% lower for the MCFe/Cr_2O_3 diffusion couple compared to the MC-Cr_2O_3 diffusion couple and the reaction layer formed in case of the MCFe/Cr_2O_3 diffusion couple contained a small, but non-negligible amount of Fe (~1 at.%). Considering grain boundary diffusion as the dominant transport mechanism, a likely explanation for the slower growth of the RL in case of the MCFe/Cr_2O_3 diffusion couple is that Fe in the grain boundaries impedes diffusion.

Assuming that the effective diffusion coefficient of Co in the RL is invariant of time and RL thickness, the diffusion coefficient may be expressed through the flux equation:

$$J_{Co} = -D_{Co}\frac{c_{Co}^{Cr_2O_3} - c_{Co}^{spinel}}{x} \quad (1)$$

where D_{Co} is the effective diffusion coefficient of Co in the RL, x is the RL thickness, and c_{Co}^{spinel} and $c_{Co}^{Cr_2O_3}$ are the molar concentrations of Co at the RL/MC(Fe) and RL/Cr_2O_3 interfaces, respectively. Assuming that $c_{Co}^{Cr_2O_3} - c_{Co}^{spinel}$ is constant (thermodynamic equilibrium at both interfaces):

$$J_{Co} = \frac{1}{V_{RL}}\frac{dx}{dt} \quad (2)$$

where V_{RL} is the molar volume of the RL. Combining Eqs. (1) and (2), and noting that $x = 0$ at $t = 0$, it may be shown by integration that:

$$x^2 = -2D_{Co}(c_{Co}^{Cr_2O_3} - c_{Co}^{spinel})V_m t = 2kt, \text{ where } k = -D_{Co}(c_{Co}^{Cr_2O_3} - c_{Co}^{spinel})V_m \quad (3)$$

The relationship $x^2 = 2kt$ is the common parabolic rate law [25]. By rearranging Eq. (3), the effective diffusion coefficient of Co in the RL can be estimated from the parabolic growth rate:

$$D_{Co} = \frac{k}{(c_{Co}^{Cr_2O_3} - c_{Co}^{spinel})V_m} \quad (4)$$

According to Eq. (4), the effective diffusion coefficient of Co is $1.2 \times 10^{-13}\,cm^2\,s^{-1}$ in the RL formed with the MC/Cr_2O_3 diffusion couple and $1.0 \times 10^{-13}\,cm^2\,s^{-1}$ in the RL formed with the MCFe/Cr_2O_3 diffusion couple.

The tracer diffusion of ^{60}Co in $CoCr_2O_4$ was previously studied by Sun [35] and Morkel and Schmalzried [37], in both cases at temperatures > 1200 °C. Extrapolation by using the reported pre-exponential factor and activation energy for Co diffusion in $CoCr_2O_4$ gives D_{Co} (900 °C) = $3 \times 10^{-13}\,cm^2\,s^{-1}$ according to data from Sun [35], which is comparable to the diffusion coefficients calculated here. The data from Morkel and Schmalzried [37] predicts a much lower diffusion coefficient of D_{Co} (900 °C) = $1 \times 10^{-15}\,cm^2\,s^{-1}$. To the best of the authors' knowledge, the only report of the diffusion coefficient in spinel oxides at 900 °C is by Gilewicz-Wolter et al. [38], measuring the tracer diffusion of ^{51}Cr ($7.2 \times 10^{-11}\,cm^2\,s^{-1}$), ^{54}Mn ($2.9 \times 10^{-10}\,cm^2\,s^{-1}$) and ^{59}Fe ($4.8 \times 10^{-12}\,cm^2\,s^{-1}$) in $MnCr_2O_4$ [38]. In this case, diffusion along grain boundaries was found to be larger than the volume diffusion. Accordingly, the scatter in the determined diffusion coefficient may, among other factors, be attributed to differences in sample grain size and density.

Wang et al. [19] studied the interaction between Cr_2O_3 and

Table 1
Parabolic growth rate of spinel reaction layers compared to literature.

Diffusion couple	Parabolic growth rate [$\mu m^2 s^{-1}$]	Reference
$Cr_2O_3/MnCo_2O_4$	1.3×10^{-5}	This work
$Cr_2O_3/Mn_{1.5}Co_{1.5}O_4$	6.9×10^{-5}	[19]
$Cr_2O_3/MnCo_2O_4$	8.6×10^{-6}	This work
$Cr_2O_3/MnCo_{1.66}Fe_{0.34}O_4$	2.9×10^{-5}	[19]

$Mn_{1.5}Co_{1.5}O_4$ spinel using an experimental set-up similar to the one discussed here. Also in their case, a Cr-rich reaction layer with a higher Co-to-Mn fraction than in $Mn_{1.5}Co_{1.5}O_4$ was observed to form at the interface with Cr_2O_3. The parabolic growth rate of this layer was $6.9 \times 10^{-5}\,\mu m^2\,cm^{-1}$ at 900 °C, which is ca. five times larger than the value we measured for the MC/Cr_2O_3.diffusion couple ($1.3 \times 10^{-5}\,\mu m^2\,s^{-1}$). Note that we have studied a more Co-rich spinel (i.e. $MnCo_2O_4$). Wang also found a beneficial effect of Fe-substitution, reporting that the parabolic growth rate of the Cr-rich RL decreased to $2.9 \times 10^{-5}\,\mu m^2\,cm^{-1}$ for a $MnCo_{1.66}Fe_{0.34}O_4/Cr_2O_3$ diffusion couple. This is ca. three times larger than the rate constant we measured for the MCFe/Cr_2O_3 diffusion couple ($8.6 \times 10^{-6}\,\mu m^2\,s^{-1}$). In this case, the spinel oxide we studied has nearly the same composition (i.e. $MnCo_{1.7}Fe_{0.3}O_4$). The comparison of the reaction rate constants is summarized in Table 1.

4.2. Reaction layer formation with MCCu

The RL formed with the MCCu/Cr_2O_3 diffusion couple consisted of two phases, namely Cr-rich grains surrounded by bands containing a relatively higher fraction Mn and Cu (Fig. 3). This type of morphology suggests a miscibility gap in the spinel solid solution [39]. The position of the Pt-markers indicates that the two-phase RL grows by diffusion of Co (and Mn/Cu) from the MCCu spinel to Cr_2O_3, i.e. the same as in the case of the MC/Cr_2O_3 and MCFe/Cr_2O_3 diffusion couples. However, based on the significantly faster growth, the diffusion rates are clearly higher in the reaction layer formed with the MCCu/Cr_2O_3 diffusion couple. According to Eq. (3), the effective diffusion coefficient of Co in the RL formed with the MCCu/Cr_2O_3 diffusion couple is $1.3 \times 10^{-12}\,cm^2\,s^{-1}$.

The position of the Pt markers indicates some diffusion of Cr from the Cr-rich reaction layer into the MCCu spinel. This suggests that Cu increases the diffusion rate of Cr in the spinel phase and that application of the MCCu material as a coating on stainless steel may not provide as efficient protection against Cr outwards diffusion as the Cu-free materials (MC or MCFe). This is in line with reports by Grolig et al. [40,41] that measured the Cr-evaporation of ferritic stainless steel with Mn-Cu, Fe-Cu, and Cu-Fe metallic coatings that are transformed to spinel oxides upon exposure to air above 800 °C. All of these Cu containing coatings were reported to be less protective than a Co coating, which is transformed to a $(Mn,Co)_3O_4$ spinel by interaction with Mn diffusing outwards from the alloy.

Small precipitates of CuO were observed both in the as-sintered and in the annealed samples of MCCu. Furthermore, a Cr-Cu-rich oxide phase formed at the interface between the $(Mn,Co,Cu,Cr)_3O_4$ reaction layer and Cr_2O_3, in particular close to the edge of the diffusion couple (Fig. S3, Supplementary Material). Based on EDX results and thermodynamics of the Cr-Cu-O system, this phase is probably $CuCrO_4$ [42]. The amount of $CuCrO_4$ was significantly higher towards the edges of the diffusion couple, where the access of oxygen is higher relative to the center. This suggests a close to atmospheric pO_2 is needed for the $CuCrO_4$ phase to form.

The MCCu/Cr_2O_3 diffusion couple results in this work are in contradiction with the results presented by Kumar et al. [43] who studied the interaction between sintered $Mn_{1.5}Co_{0.9}Cu_{0.6}O_4$ pellets and 441 type FSS, which typically forms a scale consisting of Cr_2O_3 and $(Mn,Cr)_3O_4$. No Cr-rich spinel was observed at the interface after annealing this diffusion couple for 100 h at 900 °C. The reason for these differences is likely related to the source of Cr (sintered Cr_2O_3 vs. a stainless steel containing Mn) and the differences in local pO_2 arising in these two systems. This will be further discussed in Section 4.3.

4.3. Reaction layers formed with diffusion couples vs. spinel coated steel

The diffusion couple experiments here were designed to determine the reactivity and diffusion constants in the spinel phases typically found on coated interconnect steel. We have previously reported on the formation of Cr-rich reaction layers on MC, MCFe and MCCu coated Crofer 22 APU after 2000 h aging in air at 900 °C [20]. The observations made on the spinel coated steel will in the following be compared to the results of the diffusion couple study to propose two different mechanisms for growth of the RL, illustrated in Fig. 5.

Based on the parabolic growth rate determined for the MC/Cr_2O_3 diffusion couple in the current work, the RL thickness should be ca. 9.7 ± 2.6 μm after 2000 h at 900 °C. This is nearly twice the thickness of the RL observed with MC coated Crofer 22 APU after 2000 h of oxidation at 900 °C (5.1 ± 1.5 μm) [20]. There are also other differences: in the diffusion couple, the composition of the RL is practically constant across the layer thickness (composition: $Co_{0.9}Mn_{0.2}Cr_{1.9}O_4$). In case of the MC coated alloy [20], the Cr-content and Co-to-Mn fraction in the RL gradually decreased from the interface with the thermally grown Cr_2O_3 scale towards the coating/air interface. On average, the RL formed on the coated steel contained four times more Mn compared to the RL formed with the diffusion couple (average composition: $Co_{0.9}Mn_{0.8}Cr_{1.2}Fe_{0.1}O_4$).

The differences between the coated alloy and the diffusion couple are even greater for the MCCu material. The RL formed on MCCu coated Crofer 22 APU in [20] was too discontinuous along the interface to

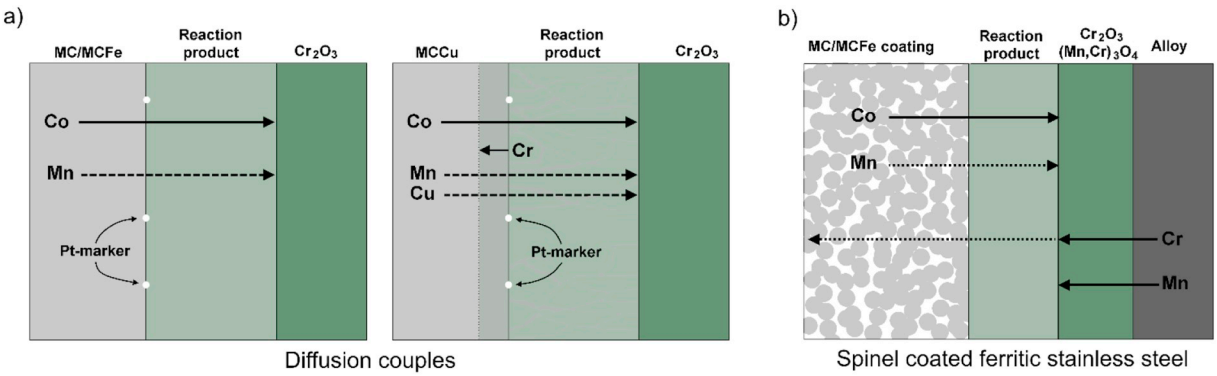

Fig. 5. Proposed reaction layer growth mechanism for the system of (a) spinel/Cr_2O_3 diffusion couples (b) Mn containing alloy coated with a spinel oxide, based on results in Ref. [20]. Note that the layer thicknesses are not to scale.

determine an average thickness, however, the RL was clearly thinner than observed here for the MCCu/Cr_2O_3 diffusion couple. Furthermore, the two-phase mixture of a Cr-rich and Cr-lean product and the formation of $CuCrO_4$ and CuO was not observed in the case of the MCCu coated alloy.

There are a number of possible explanations for the differences in the growth rate and composition of the RL formed with the diffusion couples and the RL formed with the spinel coated steel. First of all, the coating is deposited as a powder from suspension and needs to be sintered before exposure. In Ref. [20] this was done by heat treating first in N_2-H_2 at 900 °C for 2 h and then in air at 800 °C for 2 h. During the first step, the MC spinel is decomposed to MnO and Co, and during the second step the spinel phase is re-formed by reaction between these components [44,45]. After the two-step sintering heat treatment, the MCCu coating in [20] contained ca. 20 wt% Fe in a 2–3 μm layer closest to the alloy/oxide scale interface. That is, the coating effectively had a different composition than the MCCu pellet used in the diffusion couple study. The absence of any phase separation in the MCCu coating indicates that the spinel phase is stabilized by Fe. Reduction and re-oxidation of the coating may as well have led to changes in the local composition or defect chemistry of the MC and MCFe materials, affecting their reactivity with the thermally grown oxide scale.

Marker studies of the oxidation of $MnCo_2O_4$ coated E-brite have indicated that the $(Mn,Co,Cr)_3O_4$ reaction layer grows by inward diffusion of Co and Mn from the coating to the thermally grown oxide scale [46], which in line with the observations made here with the diffusion couples. However, the RL growth in the case of the coated alloy may be dictated not only by the diffusion rate of Co through the RL, but also by the diffusion rate of Cr through the thermally grown Cr_2O_3 scale. Two-stage oxidation experiments with $^{16}O/^{18}O$ have shown that the oxide scale on uncoated Crofer 22 APU mainly grows by outward transport of cations [47,48]. That is, Cr diffuses from the alloy to the Cr_2O_3/coating interface. The driving force for diffusion will depend on the defect chemistry, which is different for the two systems due to differences in the local oxygen partial pressure. In the case of the spinel coated steel, the pO_2 at the steel/Cr_2O_3 interface is equal to the dissociation pressure of Cr_2O_3, which is $\sim 10^{-24}$ atm at 900 °C. The pO2 at the coating/air interface is 0.21 atm. In the chromia scale and reaction layer the oxygen activity will vary in a complicated manner between these two values (dictated by the diffusion constants in the layers). Since oxygen is consumed by the oxidation of Cr, the pO_2 at the RL/Cr_2O_3 interface of the coated steel is much lower than the pO_2 at the RL/Cr_2O_3 interface of the diffusion couple. The concentration of Cr vacancies decreases with decreasing pO_2 [49], and accordingly, the diffusion of Cr to the RL/Cr_2O_3 interface is slower in case of the spinel coated steel than in case of the diffusion couple. The slower diffusion of Cr contributes to decrease the growth rate of the RL in case of the spinel coated steel.

Another difference is that unlike the spinel pellets, which can be considered a semi-infinite source of Co and Mn cations, the spinel coatings are relatively thin (< 20 μm). This means that the coating composition is subject to continuous change as Co and Mn cations are consumed to form the RL. The change in composition will decrease the driving force for diffusion with time for the spinel coated samples.

Finally, it is important to consider that the thermally grown oxide scale on Crofer 22 APU is not pure Cr_2O_3. The alloy contains ca. 0.4 wt % Mn and in the absence of a coating, $(Mn,Cr)_3O_4$ is typically formed on top of Cr_2O_3 [47,50]. The outward diffusion of Mn from the alloy to the scale/coating interface is a likely explanation for the relatively higher fraction of Mn in the reaction layer of spinel coated Crofer 22 APU compared to the reaction layer of the MC/Cr_2O_3 and MCFe/Cr_2O_3 diffusion couples. The higher fraction of Mn due to diffusion from the steel will have influences on the defect chemistry and thus the diffusion rate through the RL.

Gambino et al. [45] showed that during the first step of coating sintering in reducing atmosphere, $(Mn,Cr)_3O_4$ is formed as the main component of the thermally grown oxide scale on Crofer 22 APU. During subsequent oxidation, the interactions in the alloy-coating system are therefore primarily between $(Mn,Cr)_3O_4$ and the coating material. This will obviously change the thermodynamic driving force for reaction. According to Östby and Chen [30], the Gibbs energy change for the reaction $CoO + Cr_2O_3 = CoCr_2O_4$ is −53.4 kJ/mol at 900 °C. For the exchange reaction $CoO + MnCr_2O_4 = MnO + CoCr_2O_4$ the Gibbs energy change at 900 °C is −1.3 kJ/mol according to FactSage calculations [51], using literature data from [52] for MnO and $MnCr_2O_4$, and data from [30] for CoO and $CoCr_2O_4$. This means that there is a much greater thermodynamic driving force for formation of $CoCr_2O_4$ by the first reaction compared to the second.

Stainless steels specially developed for use as SOFC interconnects, such as Crofer 22 APU and ZMG232, are added small amounts of Mn to promote the formation of a continuous $(Mn,Cr)_3O_4$ scale which reduces the Cr vaporization relative to a Cr_2O_3 scale. The results here suggest that having Mn in the steel is useful also in cases when the steel is coated, as it reduces the growth rate of the Cr-rich reaction layer. Persson et al. [53] have previously reported on the importance of the steel's Mn content for the reactivity towards Co-containing coatings. In absence of Mn, a Co-containing coating was found to be too reactive towards the steel.

The proposed mechanisms for RL formation in case of the diffusion couples and the coated steel are illustrated in Fig. 5a and b, respectively. To summarize, the reaction layer in case of the MC and MCFe diffusion couples is formed by Co (and Mn) diffusion to the RL/Cr_2O_3 interface (Fig. 5a). For the MCCu diffusion couple there is additional diffusion of Cr from the RL into the spinel oxide. In case of the spinel coated ferritic stainless steel, the reaction layer is also formed by Co (and Mn) diffusion to the interface between the RL and the thermally grown oxide scale (Cr_2O_3 and $(Mn,Cr)_3O_4$). However, in this case, there is also some diffusion of Mn and Cr from the steel to this interface (Fig. 5b), which likely contributes in dictating the RL growth rate.

The existing results do not allow for an unambiguous conclusion on the main reason for the difference in reactivity between the diffusion couple and the coated steel. Nevertheless, from the foregoing discussion it is clear that an important factor must be the difference in defect chemistry due to differences in pO_2 and Mn concentration in the two systems. The effect of Mn needs to be more carefully investigated and a next step could therefore be to study diffusion couples between the MC/MCFe/MCCu spinel oxides and $MnCr_2O_4$. Finally, the effect of temperature should be considered. The annealing temperature used in this work (900 °C) is higher than the typical operating temperature of most SOFC stacks today (650–850 °C) [4,54] and was chosen to decrease the time needed to grow the reaction layers. However, since changes in the phase equilibria at lower temperatures may influence the reaction mechanism and kinetics, future work should include tests under more realistic operating conditions.

5. Conclusion

The interaction between Fe and Cu doped $MnCo_2O_4$, and Cr_2O_3 was studied at 900 °C using diffusion couples. With the pure and Fe-doped material a single reaction product with approximate composition $Co_{0.9}Mn_{0.2}Cr_{1.9}O_4$ was formed during annealing. The growth rate of this product followed parabolic kinetics, with a rate constant of $1.3 \times 10^{-5}\,\mu m^2\,s^{-1}$ for the MC/Cr_2O_3 diffusion couple and $8.6 \times 10^{-6}\,\mu m^2\,s^{-1}$ for the MCFe/Cr_2O_3 diffusion couple. In case of the MCCu/Cr_2O_3 diffusion couple, the reaction resulted in a two-phase reaction layer. The growth of this layer followed parabolic kinetics with a rate equal to $1.2 \times 10^{-4}\,\mu m^2\,s^{-1}$. Cr was observed to diffuse from the Cr-rich reaction layer into the MCCu spinel. By use of Pt-markers it was shown that the reaction layer in all three systems grew primarily by diffusion of Co (and Mn/Fe/Cu) to the reaction layer/Cr_2O_3 interface.

The thickness and composition of the diffusion couple reaction layers were significantly different from what we have previously

observed on spinel coated ferritic stainless steel after oxidation. Possible explanations for these differences were discussed. The fact that the outer oxide scale formed on most interconnect alloys is $(Mn,Cr)_3O_4$ and not Cr_2O_3 is believed to be particularly important for the slower growth of reaction layers in case of the spinel coated steel. Thus, even in the case of coated interconnects some Mn in the steel is beneficial. Another difference between the coated steel case and the diffusion couples is the effective pO_2 at the reaction layer/Cr_2O_3 interface. In the steel case this is lower than for the diffusion couples, which presumably affects the defect chemistry and thus transport properties of the phase (s).

The results of this work suggest that Cu should not be used in the spinel coating as it allows for faster diffusion of Cr. Adding Fe to the coating is on the other hand beneficial, as it slightly impedes the growth of the reaction layer.

Declarations of interest

None.

Funding

Financial support from the Faculty of Natural Sciences at the Norwegian University of Science and Technology is acknowledged.

Appendix A. Supplementary data

Supplementary data to this article can be found online at https://doi.org/10.1016/j.ssi.2019.01.008.

References

[1] S. Megel, E. Girdauskaite, V. Sauchuk, M. Kusnezoff, A. Michaelis, Area specific resistance of oxide scales grown on ferritic alloys for solid oxide fuel cell interconnects, J. Power Sources 196 (2011) 7136–7143, https://doi.org/10.1016/j.jpowsour.2010.09.003.
[2] W.Z. Zhu, S.C. Deevi, Opportunity of metallic interconnects for solid oxide fuel cells: a status on contact resistance, Mater. Res. Bull. 38 (2003) 957–972, https://doi.org/10.1016/S0025-5408(03)00076-X.
[3] K. Hilpert, D. Das, M. Miller, D.H. Peck, R. Weiß, Chromium vapor species over solid oxide fuel cell interconnect materials and their potential for degradation processes, J. Electrochem. Soc. 143 (1996) 3642–3647, https://doi.org/10.1149/1.1837264.
[4] S.P. Jiang, X. Chen, Chromium deposition and poisoning of cathodes of solid oxide fuel cells – a review, Int. J. Hydrog. Energy 39 (2014) 505–531, https://doi.org/10.1016/j.ijhydene.2013.10.042.
[5] H. Yokokawa, T. Horita, N. Sakai, K. Yamaji, M.E. Brito, Y.-P. Xiong, H. Kishimoto, Thermodynamic considerations on Cr poisoning in SOFC cathodes, Solid State Ionics 177 (2006) 3193–3198, https://doi.org/10.1016/j.ssi.2006.07.055.
[6] H. Kurokawa, C.P. Jacobson, L.C. DeJonghe, S.J. Visco, Chromium vaporization of bare and of coated iron–chromium alloys at 1073 K, Solid State Ionics 178 (2007) 287–296, https://doi.org/10.1016/j.ssi.2006.12.010.
[7] B. Talic, H. Falk-Windisch, V. Venkatachalam, P.V. Hendriksen, K. Wiik, H.L. Lein, Effect of coating density on oxidation resistance and Cr vaporization from solid oxide fuel cell interconnects, J. Power Sources 354 (2017) 57–67, https://doi.org/10.1016/j.jpowsour.2017.04.023.
[8] X. Chen, P. Hou, C. Jacobson, S. Visco, L. Dejonghe, Protective coating on stainless steel interconnect for SOFCs: oxidation kinetics and electrical properties, Solid State Ionics 176 (2005) 425–433, https://doi.org/10.1016/j.ssi.2004.10.004.
[9] S. Molin, P. Jasinski, L. Mikkelsen, W. Zhang, M. Chen, P.V. Hendriksen, Low temperature processed $MnCo_2O_4$ and $MnCo_{1.8}Fe_{0.2}O_4$ as effective protective coatings for solid oxide fuel cell interconnects at 750 °C, J. Power Sources 336 (2016) 408–418, https://doi.org/10.1016/j.jpowsour.2016.11.011.
[10] J.W. Fergus, Synergism in the design of interconnect alloy–coating combinations solid for oxide fuel cells, Scr. Mater. 65 (2011) 73–77, https://doi.org/10.1016/j.scriptamat.2010.09.020.
[11] L. Chen, E.Y. Sun, J. Yamanis, N. Magdefrau, Oxidation kinetics of $Mn_{1.5}Co_{1.5}O_4$-coated Haynes 230 and Crofer 22 APU for solid oxide fuel cell interconnects, J. Electrochem. Soc. 157 (2010) B931–B942, https://doi.org/10.1149/1.3391820.
[12] T. Horita, H. Kishimoto, K. Yamaji, Y. Xiong, M.E. Brito, H. Yokokawa, Y. Baba, K. Ogasawara, H. Kameda, Y. Matsuzaki, S. Yamashita, N. Yasuda, T. Uehara, Diffusion of oxygen in the scales of Fe–Cr alloy interconnects and oxide coating layer for solid oxide fuel cells, Solid State Ionics 179 (2008) 2216–2221, https://doi.org/10.1016/j.ssi.2008.07.024.
[13] X. Montero, F. Tietz, D. Sebold, H.P. Buchkremer, A. Ringuede, M. Cassir, A. Laresgoiti, I. Villarreal, $MnCo_{1.9}Fe_{0.1}O_4$ spinel protection layer on commercial ferritic steels for interconnect applications in solid oxide fuel cells, J. Power Sources 184 (2008) 172–179, https://doi.org/10.1016/j.jpowsour.2008.05.081.
[14] O. Thomann, M. Pihlatie, M. Rautanen, O. Himanen, J. Lagerbom, M. Mäkinen, T. Varis, T. Suhonen, J. Kiviaho, Development and application of HVOF sprayed spinel protective coating for SOFC interconnects, J. Therm. Spray Technol. 22 (2013) 631–639, https://doi.org/10.1007/s11666-012-9880-9.
[15] N.J. Magdefrau, L. Chen, E.Y. Sun, J. Yamanis, M. Aindow, Formation of spinel reaction layers in manganese cobaltite – coated Crofer22 APU for solid oxide fuel cell interconnects, J. Power Sources 227 (2013) 318–326, https://doi.org/10.1016/j.jpowsour.2012.07.091.
[16] M. Bobruk, S. Molin, M. Chen, T. Brylewski, P.V. Hendriksen, Sintering of $MnCo_2O_4$ coatings prepared by electrophoretic deposition, Mater. Lett. 213 (2018) 394–398, https://doi.org/10.1016/j.matlet.2017.12.046.
[17] Y. Liu, J.W. Fergus, C.D. Cruz, Electrical properties, cation distributions, and thermal expansion of manganese cobalt chromite spinel oxides, J. Am. Ceram. Soc. 96 (2013) 1841–1846, https://doi.org/10.1111/jace.12254.
[18] B. Talic, P.V. Hendriksen, K. Wiik, H.L. Lein, Thermal expansion and electrical conductivity of Fe and Cu doped $MnCo_2O_4$ spinel, Solid State Ionics 326 (2018) 90–99, https://doi.org/10.1016/j.ssi.2018.09.018.
[19] K. Wang, Y. Liu, J.W. Fergus, Interactions between SOFC interconnect coating materials and chromia, J. Am. Ceram. Soc. 94 (2011) 4490–4495, https://doi.org/10.1111/j.1551-2916.2011.04749.x.
[20] B. Talic, S. Molin, K. Wiik, P.V. Hendriksen, H.L. Lein, Comparison of iron and copper doped manganese cobalt spinel oxides as protective coatings for solid oxide fuel cell interconnects, J. Power Sources 372 (2017) 145–156, https://doi.org/10.1016/j.jpowsour.2017.10.060.
[21] E. Aukrust, A. Muan, Phase relations in the system cobalt oxide–manganese oxide in air, J. Am. Ceram. Soc. 46 (1963) 511, https://doi.org/10.1111/j.1151-2916.1963.tb13790.x.
[22] H. Bordeneuve, A. Rousset, C. Tenailleau, S. Guillemet-Fritsch, Cation distribution in manganese cobaltite spinels $Co_{3-x}Mn_xO_4$ ($0 \le x \le 1$) determined by thermal analysis, J. Therm. Anal. Calorim. 101 (2010) 137–142, https://doi.org/10.1007/s10973-009-0557-7.
[23] P. Hovington, D. Drouin, R. Gauvin, CASINO: a new Monte Carlo code in C language for electron beam interaction —part I: description of the program, Scanning 19 (1997) 1–14, https://doi.org/10.1002/sca.4950190101.
[24] D.R. Lide, CRC Handbook of Chemistry and Physics, CRC Press, 1992.
[25] P. Kofstad, High Temperature Corrosion, (1988).
[26] D.S. McClure, The distribution of transition metal cations in spinels, J. Phys. Chem. Solids 3 (1957) 311–317, https://doi.org/10.1016/0022-3697(57)90034-3.
[27] H.S.C. O'Neill, A. Navrotsky, Cation distributions and thermodynamic properties of binary spinel solid solutions, Am. Mineral. 69 (1984) 733–753.
[28] A.N. Hansson, S. Linderoth, M. Mogensen, M.A.J. Somers, X-ray diffraction investigation of phase stability in the Co–Cr–O and the Fe–Co–Cr–O systems in air at 1323 K, J. Alloys Compd. 402 (2005) 194–200, https://doi.org/10.1016/j.jallcom.2005.04.187.
[29] A. Naoumidis, H.A. Schulze, W. Jungen, P. Lersch, Phase studies in the chromium-manganese-titanium oxide system at different oxygen partial pressures, J. Eur. Ceram. Soc. 7 (1991) 55–63, https://doi.org/10.1016/0955-2219(91)90054-4.
[30] J. Östby, M. Chen, Thermodynamic assessment of the CoOx–$CrO_{1.5}$ system, J. Alloys Compd. 485 (2009) 427–434, https://doi.org/10.1016/j.jallcom.2009.05.135.
[31] F.-H. Lu, R. Dieckmann, Point defects and cation tracer diffusion in $(Co,Fe,Mn)_{3-\delta}O_4$ spinels: I. Mixed spinels $(Co_xFe_{2y}Mn_y)_{3-\delta}O_4$, Solid State Ionics 53–56 (Part 1) (1992) 290–302, https://doi.org/10.1016/0167-2738(92)90392-3.
[32] F.-H. Lu, R. Dieckmann, Point defects and cation tracer diffusion in $(Co,Fe,Mn)_{3-\delta}O_4$ spinels: II. Mixed spinels $(Co_xFe_zMn_{2z})_{3-\delta}O_4$, Solid State Ionics 59 (1993) 71–82, https://doi.org/10.1016/0167-2738(93)90232-R.
[33] F.-H. Lu, R. Dieckmann, Point defects and cation tracer diffusion in $(Co_xMn_{1-x})_{3-d}O_4$ spinels, Solid State Ionics 67 (1993) 145–155.
[34] J. Töpfer, S. Aggarwal, R. Dieckmann, Point defects and cation tracer diffusion in $(Cr_xFe_{1-x})_{3-\delta}O_4$ spinels, Solid State Ionics 81 (1995) 251–266, https://doi.org/10.1016/0167-2738(95)00190-H.
[35] R. Sun, Diffusion of cobalt and chromium in chromite spinel, J. Chem. Phys. 28 (1958) 290–293, https://doi.org/10.1063/1.1744108.
[36] Å.H. Persson, L. Mikkelsen, P.V. Hendriksen, M.A.J. Somers, Interaction mechanisms between slurry coatings and solid oxide fuel cell interconnect alloys during high temperature oxidation, J. Alloys Compd. 521 (2012) 16–29, https://doi.org/10.1016/j.jallcom.2011.12.095.
[37] A. Morkel, H. Schmalzried, Diffusion und fehlordnung in spinellen, Z. Phys. Chem. 32 (1962) 76–90, https://doi.org/10.1524/zpch.1962.32.1_2.076.
[38] J. Gilewicz-Wolter, J. Dudała, Z. Żurek, M. Homa, J. Lis, M. Wolter, Diffusion of chromium, manganese, and iron in $MnCr_2O_4$ spinel, J. Phys. Eqil. Diff. 26 (2005) 561–564, https://doi.org/10.1007/s11669-005-0051-2.
[39] F.J.J. van Loo, Multiphase diffusion in binary and ternary solid-state systems, Prog. Solid State Chem. 20 (1990) 47–99, https://doi.org/10.1016/0079-6786(90)90007-3.
[40] J.G. Grolig, H. Abdesselam, M. Gas, H.F. Windisch, J. Froitzheim, J.-E. Svensson, Copper based conversion coatings on ferritic stainless strip steel as solid oxide fuel cell interconnects: oxidation performance and chromium evaporation, ECS Trans. 57 (2013) 2339–2347, https://doi.org/10.1149/05701.2339ecst.
[41] J.G. Grolig, P. Alnegren, J. Froitzheim, J.-E. Svensson, Copper Iron conversion coating for solid oxide fuel cell interconnects, J. Power Sources 297 (2015) 534–539, https://doi.org/10.1016/j.jpowsour.2015.06.139.
[42] P. Perrot, Chromium – copper – oxygen, in: G. Effenberg, S. Ilyenko (Eds.), Refractory Metal Systems, Springer, Berlin Heidelberg, 2010, pp. 126–137, , https://doi.org/10.1007/978-3-642-00771-2_9.

[43] C.D. Kumar, A. Dekich, H. Wang, Y. Liu, W. Tilson, J. Ganley, J.W. Fergus, Transition metal doping of manganese cobalt spinel oxides for coating SOFC interconnects, J. Electrochem. Soc. 161 (2014) F47–F53.
[44] Z. Yang, G. Xia, S.P. Simner, J.W. Stevenson, Thermal growth and performance of manganese cobaltite spinel protection layers on ferritic stainless steel SOFC interconnects, J. Electrochem. Soc. 152 (2005) A1896–A1901, https://doi.org/10.1149/1.1990462.
[45] L.V. Gambino, N.J. Magdefrau, M. Aindow, Microstructural effects of the reduction step in reactive consolidation of manganese cobaltite coatings on Crofer 22 APU, Mater. High Temp. 32 (2015) 142–147, https://doi.org/10.1179/0960340914Z.00000000090.
[46] S.L. Tobing, High Temperature Corrosion and Corrosion Protection of Metallic Interconnects for SOFC (PhD Thesis), Norwegian University of Science and Technology, 2015.
[47] P. Huczkowski, N. Christiansen, V. Shemet, L. Niewolak, J. Piron-Abellan, L. Singheiser, W.J. Quadakkers, Growth mechanisms and electrical conductivity of oxide scales on ferritic steels proposed as interconnect materials for SOFC's, Fuel Cells 6 (2006) 93–99, https://doi.org/10.1002/fuce.200500110.
[48] S. Fontana, S. Chevalier, G. Caboche, Metallic interconnects for solid oxide fuel cell: performance of reactive element oxide coating during 10, 20 and 30 months exposure, Oxid. Met. 78 (2012) 307–328, https://doi.org/10.1007/s11085-012-9308-4.
[49] A. Holt, P. Kofstad, Electrical conductivity and defect structure of Cr_2O_3. II. Reduced temperatures (< 1000 °C), Solid State Ionics 69 (1994) 137–143.
[50] M. Stanislowski, E. Wessel, K. Hilpert, T. Markus, L. Singheiser, Chromium vaporization from high-temperature alloys I. Chromia-forming steels and the influence of outer oxide layers, J. Electrochem. Soc. 154 (2007) A295–A306, https://doi.org/10.1149/1.2434690.
[51] C.W. Bale, P. Chartrand, S.A. Degterov, G. Eriksson, K. Hack, R. Ben Mahfoud, J. Melançon, A.D. Pelton, S. Petersen, FactSage thermochemical software and databases, Calphad 26 (2002) 189–228, https://doi.org/10.1016/S0364-5916(02)00035-4.
[52] L. Kjellqvist, M. Selleby, Thermodynamic assessment of the Cr–Mn–O system, J. Alloys Compd. 507 (2010) 84–92, https://doi.org/10.1016/j.jallcom.2010.04.252.
[53] Å.H. Persson, High Temperature Oxidation of Slurry Coated Interconnect Alloys (PhD thesis), Technical University of Denmark, 2007, http://forskningsbasen.deff.dk/Share.external?sp=Sfa1de473-3a68-4546-bc1d-60d4621072b4&sp=Sdtu , Accessed date: 22 October 2015.
[54] N. Shaigan, W. Qu, D.G. Ivey, W. Chen, A review of recent progress in coatings, surface modifications and alloy developments for solid oxide fuel cell ferritic stainless steel interconnects, J. Power Sources 195 (2010) 1529–1542, https://doi.org/10.1016/j.jpowsour.2009.09.069.